Water Science & Technology

IWA PUBLISHING

Water Science & Technology Vol 87 No 3, 620 doi: 10.2166/wst.2022.424

Thiabendazole degradation by photo-NaOCl/Fe and photo-Fenton like processes, using copper slag as an iron catalyst, in spiked synthetic and real secondary wastewater treatment plant effluents

Reyna García-Estrada, Sandra Arzate and Rosa-María Ramírez-Zamora *

Coordinación de Ingeniería Ambiental, Instituto de Ingeniería, Universidad Nacional Autónoma de México, Circuito Escolar s/n, Ciudad Universitaria, Coyoacán, Ciudad de México 04510, México
*Corresponding author. E-mail: rramirezz@iingen.unam.mx

SA, 0000-0002-1522-693X; R-MR-Z, 0000-0003-1129-4385

ABSTRACT

Thiabendazole degradation (TBZ_D) in diferent types of water matrices was assessed by applying two Advanced Oxidation Processes, both using simulated solar light (SSL), copper slag (CS) as an iron based catalyst, and separately H_2O_2 or NaOCl as oxidants. First, optimum conditions for TBZ_D were evaluated in distilled water, $TBZ_D = 90\%$ at 60 min for CS-H_2O_2-SSL, and 92% of TBZ_D in a twelfth of the time by the system CS-NaOCl-SSL; minimum TBZ depletion variations were observed between the first and the fifth reuse test: 88 ± 2% for CS-H_2O_2-SSL (60 min) and 90 ± 1% for CS-NaOCl-SSL (5 min). Those conditions were tested using a synthetic (SE) and a real secondary effluent (RE) from a wastewater treatment plant. The CS-H_2O_2-SSL system achieved TBZ_D of 88 and 77% after 90 min for SE and RE, with kinetic constants of 0.024 and 0.016 min^{-1}, respectively, whereas photo-NaOCl/Fe showed values of 0.365 and 0.385 min^{-1} for SE and RE, achieving a 94% TBZ_D removal in both types of water at 10 min. That might be related to the formation of $Cl^{\cdot}$ and $HO^{\bullet}$ during the photo-NaOCl/Fe process, highlighting that the CS-NaOCl-SSL is an attractive option that has great possibilities for scaling up by a better knowledge in real aqueous matrices.

Key words: fungicide, heterogeneous photo-Fenton, liquid chromatography, pollutant degradation, raceway pond reactor, water matrix

HIGHLIGHTS

- Copper slag was successfully used as catalyst in two photo assisted iron based AOPs.
- 90% TBZ degradation was achieved with the Fe based AOPs in a WWTP secondary effluent.
- Rate constant of photo/Fe/NaOCl system was three orders of magnitude larger than with H_2O_2.
- 94% TBZ removal was reached at 10 min in a WWTP secondary effluent by the photo-Fe/NaOCl.
- Nitrates and chlorides reduced the reaction rate of the photo-Fe/ H_2O_2 system by 30%.

GRAPHICAL ABSTRACT

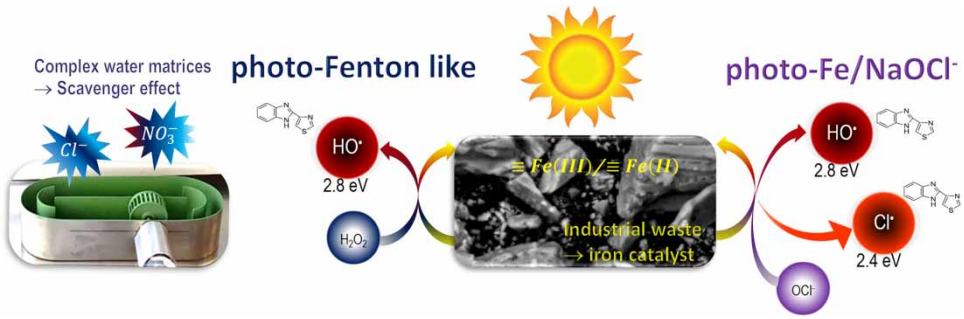

INTRODUCTION

The photo-Fenton process has been extensively studied for the degradation of recalcitrant organic contaminants in effluents of wastewater treatment plants (Ameta *et al.* 2018; Contreras-Bustos *et al.* 2019). In fact, several engineering-scale demonstration plants have been erected in order to exhibit the potentiality of the installation of this technology at full scale (Contreras-Bustos *et al.* 2019; Gualda-Alonso *et al.* 2022). One of the reasons why this technology is attractive is its capability of using solar light as a source of UV radiation, instead of lamps, and in this way, diminishing the energetic consumption (Cabrera-Reina *et al.* 2014; Hassani *et al.* 2021). Though, some drawbacks related to the pH dependency of the process, when it is performed in homogeneous systems, and the cost of the oxidant have pointed out the need to diversify operation strategies.

Thus, the implementation of a Fenton-like catalyst seems to be a good option to solve the pH drawback, due to the large pH operation range of these materials (Lima *et al.* 2017). Diverse iron-based compounds have been tested in photo-Fenton applications, like nanomaterials (nanoparticles and nano-zero-valent iron) (Carraro *et al.* 2018; Zhu *et al.* 2019; Ahmadi *et al.* 2021) and natural minerals (magnetite (Fe_3O_4), goethite (αFeOOH), maghemite (γFe_2O_3) and hematite (αFe_2O_3) (Zhu *et al.* 2019).

Nevertheless, thinking on avoiding complex chemical synthesis and considering that some industrial wastes have similar characteristics to those of natural minerals, copper slags (CS) have been successfully utilized as a Fenton-like catalyst in the degradation process of various organic pollutants and pathogens (Solís-López *et al.* 2014; Arzate-Salgado *et al.* 2016). This is because they are composed mainly of iron oxides (Solís-López *et al.* 2014) that exhibit photo-activity under visible-light irradiation due to their mineralogical phases and band gap values (Arzate-Salgado *et al.* 2016). Also, the metallurgical slags are highly dense, and that allows an easy separation, in contrast to other nanoparticles that require an additional treatment step like coagulation to separate the nanoparticles from the treated effluent (Ghanbari *et al.* 2020). Hence, use of this material as a Fenton-like catalyst also includes the possibility to face two environmental problems at the same time: the water treatment and the industrial by-products disposal, since CS is produced in abundance, approximately 2 tons per ton of produced copper (Kim *et al.* 2013), and it represents an important environmental problem to attend to.

However, it is important to mention that this material, like the majority of heterogeneous catalysts, has been commonly evaluated in distilled water. Nevertheless, it has been reported that the presence of ions and organic matter in water matrices diminishes the effectivity of pollutant degradation (Tokumura *et al.* 2016; Lado Ribeiro *et al.* 2019); for this reason, the assessment of their effectivity in synthetic and real water matrices is an important step to understand the feasibility of the process proposed.

Regarding the oxidant, the use of chlorine instead of H_2O_2 has been proposed recently (Portilla-Sangabriel *et al.* 2021). The results show that a system composed of the magnetic fraction of a low-grade titanium ore (MFTO), NaOCl and simulated sunlight (SSL), MFTO-NaOCl-SSL, halves the reaction time necessary to degrade 97% of thiabendazole (TBZ) ($TBZ_0 =$ 37 μM) in distilled water. The successful degradation of thiabendazole by the MFTO-NaOCl-SSL is related to the production of strong radicals like chlorine radicals ($Cl^{\bullet}$ (2.4 eV)), hydroxyl radicals ($HO^{\bullet}$ (2.8 eV)), $Cl_2^{\bullet -}$ (2.0 eV) and $ClO^{\bullet}$ (1.4 eV) (Armstronga *et al.* 2013; Guo *et al.* 2017), whose formation is explained in the supplementary material (Section S.1).

In this context, this work aims to assess the degradation of thiabendazole using two Advanced Oxidation systems composed by CS-oxidant-SSL, the oxidants being H_2O_2 (CS-H_2O_2-SSL, photo-Fenton-like) and NaOCl (CS-NaoOCl-SSL, photo-NaOCl/Fe), in three aqueous matrices: distilled, synthetic, and real secondary effluent from a wastewater treatment plant (WWTP).

MATERIALS AND METHODS

Reagents

Sodium hypochlorite (5.25% w/w) was purchased from Golden Bell. Hydrogen peroxide (30% w/w), sulfuric acid, sodium hydroxide (ACS grade) and $MgSO_4{\cdot}7H_2O$ were acquired from J.T. Baker. N-Diethyl phenylenediamine was bought from Hach. Thiabendazole (>99%), beef extract (>90%), sodium thiosulphate (0.1 N), titanium (IV) oxysulfate solution (1.9–2.1%), phosphoric acid (85%), acetonitrile and water HPLC grade were supplied by Sigma–Aldrich. NaCl (95%), $CaSO_4{\cdot}2H_2O$ (98%), $MgSO_4$ (>98%), KCl (>99%), $CaCl_2{\cdot}H_2O$ (>99%), urea (>99%) and $NaHCO_3$ (95–100%) were provided by Meyer. Finally, peptone was acquired from Lab (Grade for Bacteriology).

Metallurgical copper slag

A metallurgical copper slag sample, issued from a northern Mexican smelter, was milled and sieved; the fraction with a particle size between 180 and 250 μm (60–80-mesh) was used in this study. CS characterization was previously reported by our group in the works of Solís-López *et al.* (2014); Arzate-Salgado *et al.* (2016) and García Estrada *et al.* (2020). Briefly, scanning electron microscopy (SEM) images were recorded to identify the morphology of CS (Philips XL20 SEM equipped with an Oxford 7593 solid state energy-dispersive X-ray (EDX) detector). The phase composition of the solid phase was determined by X-ray diffraction (XRD) on an Empyrean diffractometer with focused Cu-Kα radiation and a Ni filter in a 2θ interval from 4° to 70° in steps of 0.003° at 40 s per step. And XRD was used for the identification of the mineral phases. The chemical composition was determined by X-ray fluorescence (XRF) using an SRS 3X00 sequential X-ray spectrometer. The band gap of the CS was determined by applying the Tauc-plot method, considering direct interactions and using the UV-vis diffuse reflectance spectroscopy technique (UV-Vis-DRS) with a Cary 500 UV/vis/near infrared (NIR) spectrophotometer (Varian Inc.). The surface area of CS was determined by the adsorption-desorption of N_2 gas in a Bel-Sorp mini II apparatus (Belsorp Inc., Japan) using the BET (Brunauer-Emmett-Teller) isotherm methodology.

Water matrices

Three different aqueous matrices were used to run the experiments: distilled water, synthetic effluents and real secondary effluents from WWTPs. All of them were spiked with thiabendazole as model pollutant. TBZ is a fungicide usually used during postharvest storage to preserve fruits and vegetables. It has been used as a model pollutant because it is highly recalcitrant; in fact, concentrations of 0.11–70 μg/L have been found in wastewater treatment plant effluents (Bernabeu *et al.* 2011).

Distilled water used to prepared TBZ solutions was produced *in situ* and complies with Type II water characteristics, according to ASTM D1193–99e1 (ASTM 1999), with resistivity of >1 MΩ-cm, a conductivity of <1 μS/cm and <50 ppb of total organic carbon (TOC).

Synthetic effluent (SE) was prepared using the composition reported by Klamerth *et al.* (2010), which represents the effluent from aerobic sewage treatment according to OECD Guidelines (OECD 2001). Real effluent (RE) was collected in the downstream tank of activated sludge, a secondary treatment from the WWTP Cerro de la Estrella, located on the southeast side of Mexico City, Mexico. The main features of both synthetic and real effluents are shown in Table 1.

Considering that carbonates (HCO_3^-/CO_3^{2-}) present in the secondary effluents act as radical scavengers (Pignatello *et al.* 2006), a concentration of 15 mg/L, expressed as Total Inorganic Carbon (TIC), was set in both matrices; in SE, the concentration was adjusted by the addition of $NaHCO_3$, while in RE, a stoichiometric amount of sulfuric acid was added, under agitation, to strip the carbonates.

Analytical techniques

High-performance liquid chromatography (HPLC) was used to measure TBZ concentration in water, using a 1100 Agilent chromatography apparatus equipped with a photo-diode array detector (Agilent) and an HPLC column ACE5 C18-AR (150 mm × 4.6 mm). The mobile phase was a mixture of methanol, acetonitrile, and phosphoric acid (0.1%, v/v) at a

Table 1 | Characterization of water matrices

Parameter	Real effluent	Synthetic effluent
COD (mg/L)	22	51
BOD_5 (mg/L)	10	25
DOC (mg/L)	19	17
Cl^- (mg/L)	56	8
NO_3^- (mg/L)	265	53
SO_4^{2-} (mg/L)	3	3
pH (-)	7.34	7.94
Conductivity (μS/cm)	846	298
Turbidity (NTU)	0.8	1.7

10:8:82 ratio (v/v), pumped at a flow rate of 1.0 mL/min. The sample volume of injection was 30 μL and TBZ was detected at a wavelength (λ) of 270 nm. The limit of detection (LOD) was 100 μg/L (4.97×10^{-1} μM).

Oxidant concentrations were measured throughout each experiment; hydrogen peroxide concentration was determined with the DIN 38 402 H15 colorimetric method using a titanium (IV) oxysulfate solution; while the NaOCl content was quantified by measuring free chlorine concentration with an HI 96701 Free Chlorine device (ISM-HANNA Instruments), which adapts the USEPA method 330.5 and Standard Method 4500-Cl G.

Total leached iron concentration was measured using the Merck Kit (Spectroquant 1.14761.001) with an LOD of 0.3 mg/L, at the end of each experiment. The method implies the reduction of all the iron species in dissolution to Fe^{2+}, in a thioglycolate-buffered medium, to react with a triazine to form a red-violet complex.

Chemical oxygen demand (COD) was determined according to the standardized method 5220 D (AWWA/APHA/WEF 2012); the acid digestion was run in a COD digester, and the spectrophotometric measurement was made in a HACH LANGE DR/4000 U, UV-VIS Spectrophotometer. Biochemical oxygen demand (BOD_5) was measured using a Respirometric OxiTop measuring system, which follows the standardized method 5210 (AWWA/APHA/WEF 2012). Dissolved organic carbon (DOC) and inorganic carbon analysis were performed using the standardized method 5310B (AWWA/APHA/WEF 2012) with a TOC analyser (Shimadzu TOC-L CSN). Ion chromatography (Thermo Scientific Dionex) was used for measuring the concentration of anions. Conductivity and pH were measured with a Benchtop Meter (Thermo Scientific Orion Versa Star); and turbidity was quantified using a Merck Turbiquant.

Experimental setup

The oxidation experiments were performed using SSL provided from a Xenon lamp (400–800 nm), with 5–6% photon emissions between 290 and 400 nm. The profile of the emitted photons between 400 and 800 nm at a light intensity simulates the solar spectrum. The lamp is installed inside a solar simulator chamber (SUNTEST CPS + ATLAS) (Figure 1(a)), as previously described in Arzate-Salgado *et al.* (2016). A Raceway Pond Reactor (RPR) of 1 L capacity (Figure 1(b)) was operated at 5 cm liquid depth; its dimensions are length of 0.27 m and width of 0.10 m (Portilla-Sangabriel *et al.* 2021).

In all the experiments, the light intensity was set constant at 400 W/m^2, in order to simulate the global solar radiation in Mexico (hours of sunlight) (Almanza & López 1978).

Optimization of operating conditions

A central composite experimental design was used to determine the optimum values of CS and oxidant doses for the CS-H_2O_2-SSL and CS-NaOCl-SSL systems for a given initial concentration of thiabendazole (TBZ_0) in distilled water; this procedure is explained in detail in the supplementary material (Section S.2.1). The optimum values obtained were tested in five reuse cycles. CS was separated from the treated effluent by settling, because of its high density; then the catalyst was placed in tubes with water, stirred and centrifuged at 500 rpm for 10 min; the supernatant was decanted, and the sediment was re-suspended in water (Arzate-Salgado *et al.* 2016). Then the CS was dried at 105 °C before each cycle.

Related micropollutant (MP) removal mechanisms

Considering that the experimental systems are composed of three elements, CS, oxidant and SSL, several mechanisms that involve just one or two of them may occur during the reaction; thus, in order to clarify the contribution of each mechanism to

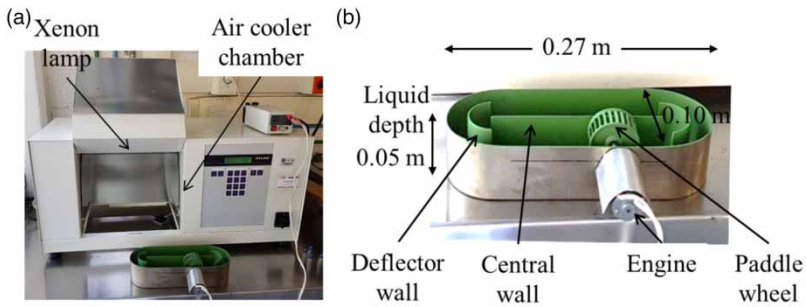

Figure 1 | Reaction system for the TBZ photocatalytic degradation tests: (a) solar simulator chamber and (b) Raceway Pond Reactor.

MP removal, control experiments were carried out, conserving the optimum values of factors determined with the statistical second-order model. Table 2 shows the mechanism analysed and the value of each factor.

TBZ degradation in complex water matrices

Experiments in synthetic and real WWTP secondary effluents were carried out. In both cases, TBZ initial concentration was adjusted to 7.36 mg/L in order to appraise better its concentration changes. CS and oxidant doses were set up by using the response surface graphs, looking for an oxidant/TBZ ratio that complied with 90% degradation and less oxidant consumption; in this way, 1.11 g CS and 50 mg H_2O_2/L or 98 mg NaOCl/L were used in the systems CS-H_2O_2-SSL and CS-NaOCl-SSL, respectively. Tests were run in triplicate.

In the sequence, reaction order was determined, and rate constants were calculated. Since TBZ degradation exhibited a pseudo-first-order reaction, the value was estimated using Equation (1); where k' is the pseudo-first-order rate constant, C_0 the initial concentration, C is the concentration at time t.

$$ln\frac{C}{C_0} = k't \tag{1}$$

RESULTS AND DISCUSSION

Copper slag characterization

A detailed description of the copper slag characterization is available in Solís-López *et al.* (2014), Arzate-Salgado *et al.* (2016) and García Estrada *et al.* (2020).

Briefly, the morphologies of CS samples obtained by SEM are shown in Figure 2. The sample is composed by small particles with angular shape; in the surface of the material large cavities are observed without an apparent pattern. The images show a non-porous material. This observation is in line with the superficial area 14.94 m^2/g (Solís-López *et al.* 2014), which allows us to expect low contaminant adsorption on the surface of the material (Carmalin & Eder 2018) and limitations on the production of $HO^{\cdot}$ by heterogeneous catalyst when the material is exposed to light (Larralde *et al.* 2019).

Nevertheless, since the CS surface has a high amount of iron in the surface, 55.82% as Fe_2Ox (Table 3), another mechanism like the heterogeneous Fenton can lead to radical formation (Appendix A.1, supplementary material).

The major mineralogical phase present in the CS is fayalite (Fe_2SiO_4) (Solís-López *et al.* 2014). For this reason, this material shows a band gap of 2.20 eV; this value is associated with the main crystalline phase and allows its activation under visible-light irradiation (García-Muñoz *et al.* 2016).

Optimization of operating conditions

The models presented in Equations (2) and (3) were obtained by the optimization procedure and statistical analysis described in A.2.2. They were solved, and experiments were carried out to verify the values of TBZ_D. Figure 3 shows experimental

Table 2 | Factor values of the control assays for TBZ degradation

	Factor			
Mechanism	**TBZ_0 (mg/L)**	**CS (g/L)**	**Oxidant (mg/L)**	**SSL (W/m^2)**
Adsorption	2.01	1.17	–	–
Photolysis	2.01	–	–	400
Heterogeneous photocatalysis	2.01	1.17	–	400
Chemical oxidation (H_2O_2)	2.01	–	29.7	–
Heterogeneous Fenton-type	2.01	1.17	29.7	–
Chemical oxidation photo assisted (H_2O_2-SSL)	2.01	–	29.7	400
Chemical oxidation (NaOCl)	1.23		70.1	–
Heterogeneous oxidation (Fe/NaOCl)	1.23	1.11	70.1	–
Chemical photo assisted oxidation (NaOCl-SSL)	1.23	–	70.1	400

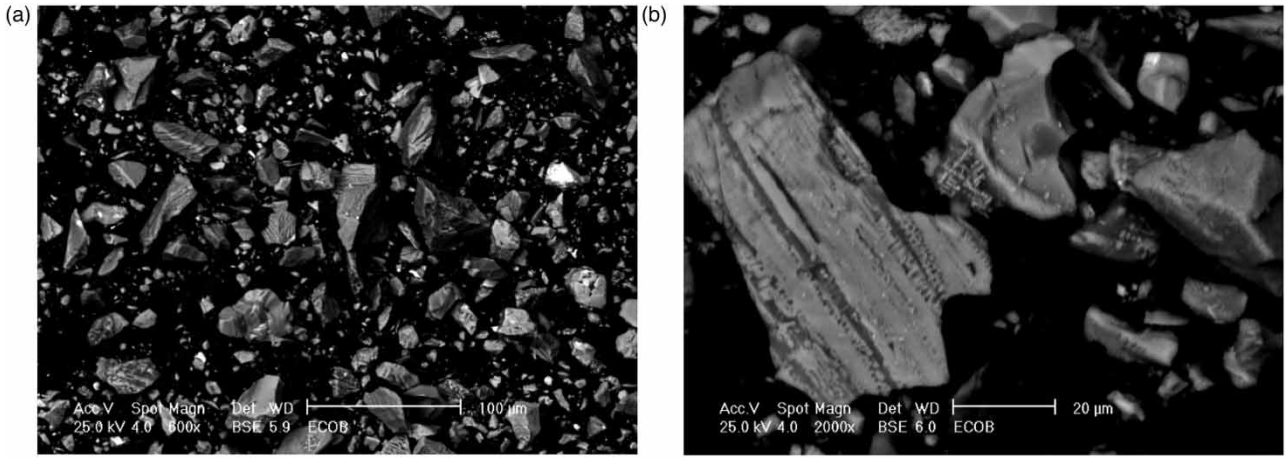

Figure 2 | Micrographs recorded using a LABE detector (low-angle electron backscattered detector, low angle backscattered electrons) by SEM. (a) Slag particles captured at a magnification of 600× and (b) 2000 × .

Table 3 | Chemical composition of CS determined by XRF (first published by García Estrada *et al.* (2020))

Compound	Wt. % ($n = 4$)
Fe_2O_3	59.26 ± 2.56
SiO_2	26.34 ± 1.54
Al_2O_3	4.2 ± 0.51
SO_3	1.33 ± 0.16
K_2O	1.15 ± 0.03
CaO	0.46 ± 0.02
TiO_2	0.31 ± 0.03
Na_2O	0.28 ± 0.04
MgO	0.30 ± 0.02
P_2O_5	0.03 ± 0.01
MnO	0.05 ± 0.01

kinetics of TBZ and oxidant concentrations in function of reaction time for the systems CS-H_2O_2-SSL (photo-Fenton like) (2) and CS-NaOCl-SSL (photo-Fe/NaOCl) (3), carried out under optimum conditions.

$$\begin{aligned} TBZ_{D-H_2O_2} &= 90.1762 + 0.9317\,H_2O_2 - 1.3424\,CS - 5.6541\,TBZ_0 \\ &\quad - 0.03450\,H_2O_2^2 + 0.176875\,H_2O_2\,CS + 0.4360\,H_2O_2{*}TBZ_0 \\ &\quad + 2.7723\,CS^2 - 2.7388\,CS{*}TBZ_0 - 0.9830\,TBZ_0^2 \end{aligned} \quad (2)$$

$$\begin{aligned} TBZ_{D-NaOCl} &= 58.0316 + 1.3283\,NaOCl - 3.4435\,CS - 9.4210\,TBZ_0 \\ &\quad - 0.0078\,NaOCl^2 + 0.0826\,NaOCl{*}CS + 0.0108\,NaOCl{*}TBZ_0 \\ &\quad - 1.8922\,CS^2 + 1.1725\,CS{*}TBZ_0 + 0.2545\,TBZ_0^2 \end{aligned} \quad (3)$$

It is evident that the TBZ degradation is faster when NaOCl is used instead of H_2O_2, showing that the first system allows an efficiency of 92% at 5 minutes, while the time in the second system should be increased 12 times to achieve 90% TBZ_D. Besides, the TBZ degradation was >99.9% at 7.5 min and 97% at 90 min for the systems CS-NaOCl-SSL and CS-H_2O_2-SSL, respectively. A similar tendency is followed by the oxidant concentration; free chlorine is not observed at

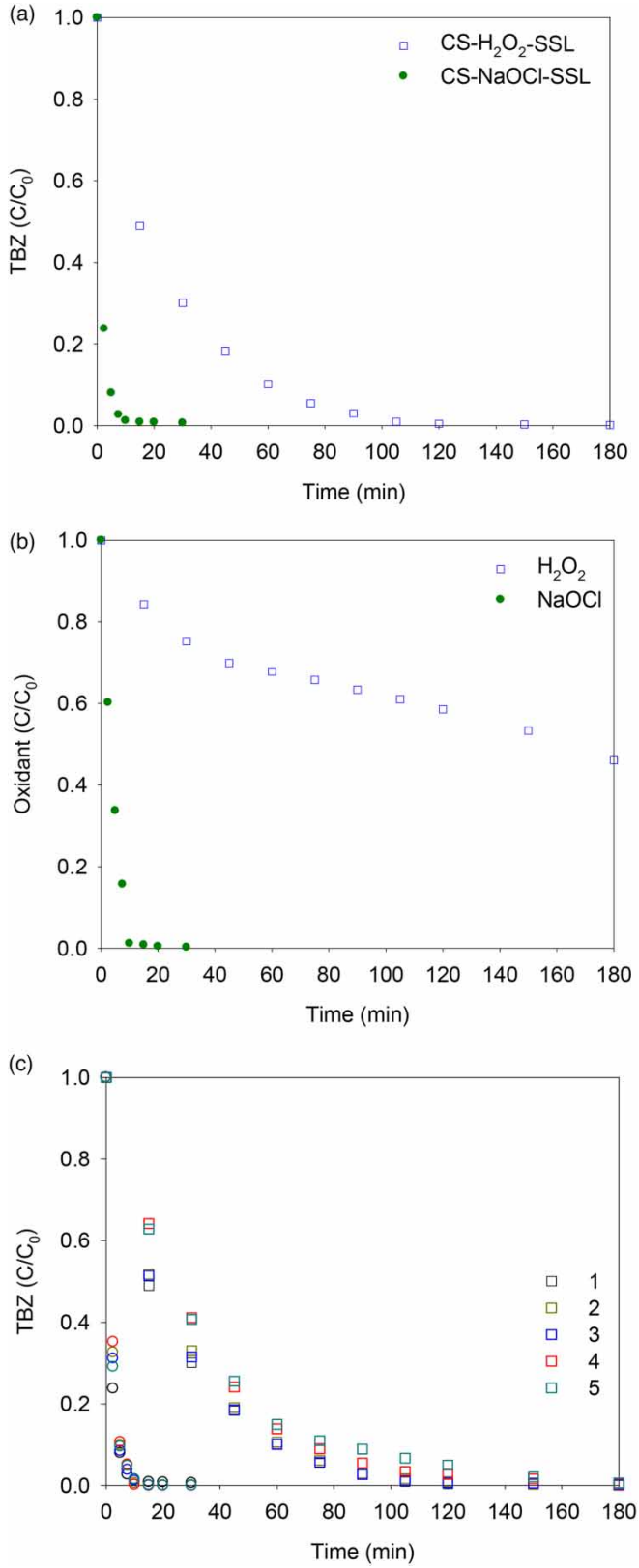

Figure 3 | TBZ degradation kinetics (a) and oxidant consumption (b) using the systems CS-H_2O_2-SSL (blue square) and CS-NaOCl-SSL (green circle), (c) reuse cycles for the TBZ degradation kinetics using the systems CS-H_2O_2-SSL and CS-NaOCl-SSL.

10 min of reaction, whereas H_2O_2 showed a slow conversion, and even at 180 min, 46% of the initial concentration remains in the reactor.

On one hand, the difference in the degradation is related to the reactivity of the radicals produced in each system. By the action of SSL, both oxidants may produce hydroxyl radicals (2.8 eV) (reactions A.4, A.5, explained in Appendix A.1, supplementary material), but chlorine radical (2.4 eV) is also produced when NaOCl is illuminated (Kong *et al.* 2016); whereby the CS-NaOCl-SSL system has this advantage over the CS-H_2O_2-SSL. On the other hand, photolytic decomposition of H_2O_2 occurs at 200–280 nm (Georgiou *et al.* 2002), while for the aqueous chlorine, decomposition is observed at 320 and 340 nm (Nowell & Hoigni 1992); thus, considering the distribution of the sunlight spectrum, the reaction using chlorine species is more favoured.

$$HOCl/OCl^- + \lambda \rightarrow HO^\bullet/O^{\bullet -} + Cl^\bullet \quad (4)$$

$$H_2O_2 + \lambda \rightarrow 2HO^\bullet \quad (5)$$

Additionally, the reaction between ferrous ion and NaOCl has been reported to be three orders of magnitude faster in comparison with H_2O_2 in homogeneous reactions (Behin *et al.* 2017). Even though there are no reports that measure the reaction of Fe^{2+} and NaOCl in heterogeneous systems, a faster reaction between them in comparison with Fenton-like reaction is expected, because the speed of the catalytic decomposition of H_2O_2 in the presence of iron species depends on the oxidation state of this metal (Neyens & Baeyens 2003; Sandoval-González *et al.* 2021).

Thus, concerning TBZ degradation (Figure 4), Portilla Sangabriel *et al.* (2022) elucidated the transformation products (TPs) according to the oxidant used, H_2O_2 or NaOCl (Figure 4). When the catalyst-NaOCl-sunlight system was used only four TPs were detected, in two reaction routes: (1) the breaking of the thiazole ring, which generates TP161 and TP162. Then the $HO^\bullet$ radical attack on the C1′ and the consequent C–C chain breakage form benzimidazole (TP118), also seen in TBZ degradation by photolysis (Murthy *et al.* 1996) and heterogeneous photocatalysis (Calza *et al.* 2003). But due to the high velocity of the reaction, TP 161 is not observed, unlike the heterogeneous photo-Fenton system; and (2) the formation of TP127 and TP128

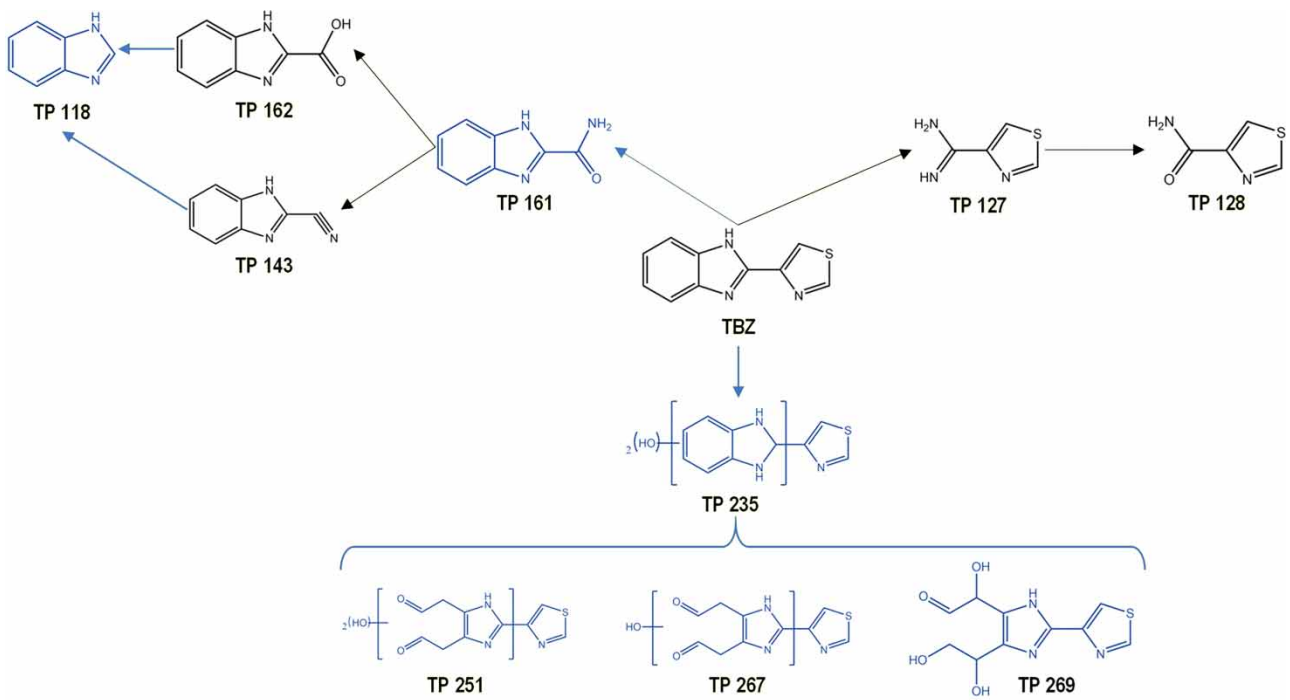

Figure 4 | Tentative transformation pathway of TBZ degradation: black intermediates occur when the system is composed of catalyst-NaOCl-light and the blue ones for MFTO-H_2O_2-light.

for the possible direct breakage of the TBZ molecule by the two N atoms in the imidazole ring. This reaction route is observed in both systems.

Then, a third reaction route is observed for the heterogeneous photo-Fenton. It starts by the formation of the TP235 by the addition of $HO^{\bullet}$ to the benzene ring by electrophilic substitution of two hydrogen atoms. Then, the benzene ring is opened, and new bonds with hydrogen and oxygen molecules are generated, forming TP251, TP267, and TP269 (Sirtori *et al.* 2014). Those TPs may lose their aliphatic chains and can be considered an intermediate step in the formation of TP127 and its subsequent oxidized derivative TP128, according to Calza *et al.* (2003). Nevertheless, a direct breakage of the TBZ molecule by the two N atoms in the imidazole ring could also generate these two TPs, because these sites are likely to be attacked by $HO^{\bullet}$ radicals due to their high electron density (Ji *et al.* 2013).

On another aspect and considering the importance of the reuse cycle of a catalyst, five repetitions using optimum conditions were performed to determine if there is any difference in MP degradation when CS is reused. Figure 3(c) presents the TBZ degradation kinetics using normalized MP concentrations for each reaction cycle. In both systems, dispersion of data is observed during the first minutes, but such difference is diminished as the reaction advances and loses speed.

Results of the CS-NaOCl-SSL system presented low dispersion in the points from 5 to 30 min, while for CS-H_2O_2-SSL two groups of data during the first 30 min (TBZ_D 64 $\pm$ 5%) can be observed, followed by irrelevant differences until the end of the reaction. Consequently, the degradation time required to achieve degradations up 80% (>45 min) is similar (standard deviation of 3%) regardless of the number of the number of times that CS is used, from one to five cycles, which is a satisfactory value according to other bench-scale studies (Bel Hadjltaief *et al.* 2014; Omri *et al.* 2020).

Related MP removal mechanisms

Figure 5 presents the kinetics of TBZ degradation using normalized TBZ concentrations corresponding to the removal mechanisms that may occur by one or the combination of two of the factors of the system. Photo-assisted oxidations (H_2O_2-SSL and NaOCl-SSL) present the best performances with respect to the rest of the mechanisms, achieving 92% of TBZ degradation at 75 min when the oxidant is H_2O_2 and 97% at 7.5 minutes when NaOCl is used instead, which fits with the kind of radicals produced by the photolysis of each oxidant. Complete degradations were achieved at 105 and 20 min using SSL with H_2O_2 or NaOCl, respectively; these reaction times are longer than data of CS-H_2O_2-SSL and CS-NaOCl-SSL.

Photolysis only contributed to 30% of TBZ degradation after 180 min due to the high stability of this contaminant (da Costa *et al.* 2019). A slight improvement of 4% by heterogeneous photo-catalysis was observed, reinforcing the idea that iron oxides are not the best semiconductors for this kind of process, since the recombination of the electron-hole pair is fast (Bin *et al.* 2018), and the porosity exhibits low values in the order of 14.94 m^2/g (Solís-López *et al.* 2014), which is responsible for the 5% of TBZ removal by adsorption.

Experiments carried out in darkness showed lower degradations, since only 11% of TBZ degradation was achieved by chemical oxidation with NaOCl and Fe/NaOCl at 30 min; while, at the same time, 3% of degradation was observed by oxidation with H_2O_2 and Fenton reaction, indicating again a higher reactivity of NaClO in contrast with H_2O_2. However, it is

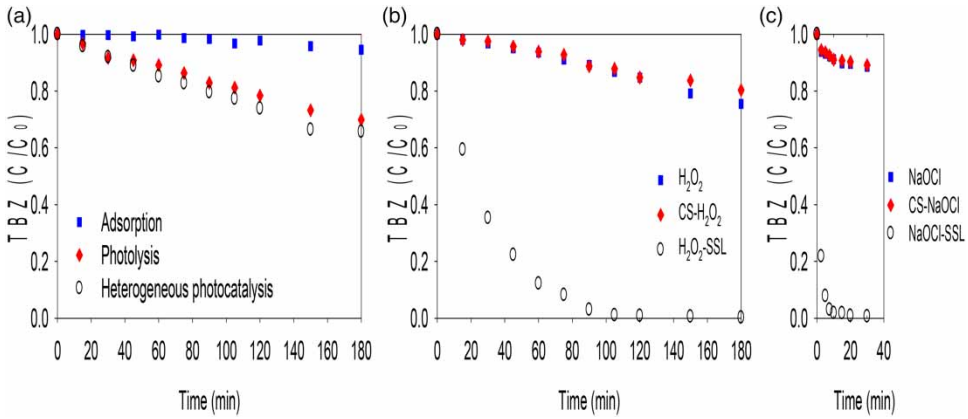

Figure 5 | TBZ degradation kinetics during control assays: (a) processes without oxidant, and processes related to (b) H_2O_2 and (c) NaOCl.

also worth mentioning the importance of SSL in the degradation mechanism to accelerate MP degradation (Zhang *et al.* 2019).

TBZ degradation in complex water matrices

Subsequently, systems composed of three elements were tested in a synthetic and a real WWTP secondary effluent. The composition between both effluents is different, as observed in Table 1; real effluent has higher concentrations of Cl^- and NO_3^- and lower contents of COD and BOD_5 in comparison whit the synthetic effluent, while COD/BOD_5 ratios are similar in both effluents (RE 2.2 and SE 2.0). The differences between the concentrations of some parameters are because the composition of the synthetic effluent corresponds to medium values of effluents issued from aerobic sewage treatment, according to OECD Guidelines (OCED 2001). Such effluents came from different WWTP installations, which do not necessarily follow the same operation strategy, but more importantly, influent compositions are not similar around the world; consequently, the sample from a real WWTP differs in some characteristics (Pescod 1992).

Despite this, the composition of such a synthetic effluent was frequently used to evaluate the performance of the photo-Fenton process in complex water matrices, having a constant composition throughout the experimentation (Klamerth *et al.* 2009). In this work, its use has been proposed in order to give an idea of how the scavenger effect of a more complex matrix, especially inorganic ions, impacts on TBZ degradation, bearing in mind that the degradation observed in distilled water may not be achieved in real applications (Loures *et al.* 2013). In fact, some studies have pointed out that ions naturally present in WWTP secondary effluents, like HCO_3^-, SO_4^{2-}, NO_3^- and Cl^-, could act as both radical scavengers and radical promoters (Gultekin & Ince 2004; Zhang *et al.* 2017).

The TBZ degradation kinetics rates using normalized MP concentrations are shown in Figure 6(a) and 6(c). For the system CS-H_2O_2-SSL, MP removal was slower in RE, with degradations of 61% at 60 min, in comparison with 75% attained in SE; then, by extending the reaction time until 90 min, the degradation values increased to 88 and 77% for SE and RE, respectively. The difference in the speed of MP removal in synthetic and real matrices was expected, due to the differences of the chemical complexity in each matrix. A similar observation was pointed out by de la Obra *et al.* (2017), who have mentioned that real effluents show a much more complex chemical composition than simulated effluents, and thus, the scavenger effect must be major.

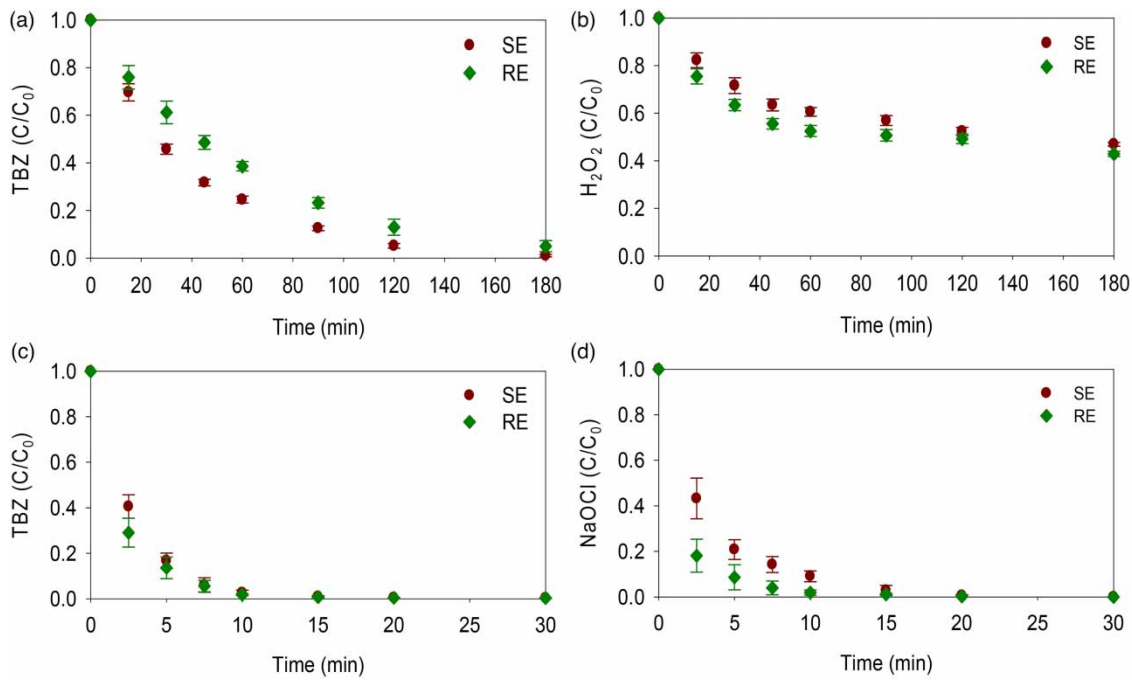

Figure 6 | Effect of the water matrix on the TBZ degradation kinetics, by the systems (a) CS-H_2O_2-SSL and (c) CS-NaOCl-SSL, and oxidant consumption (b) H_2O_2 and (d) NaOCl.

In contrast, the effect of water matrix was hardly evident during the first 7.5 min in the CS-NaOCl-SSL system; at that time, the TBZ degradation was only affected by 3%, the efficiencies being 83 and 86% on synthetic and real effluents, respectively; after 10 min of reaction time, TBZ_D was 94% in both matrices. As oxidant consumption was slightly faster in RE than SE (Figure 6(b) and 6(d)), the water matrix contributed more to oxidant consumption in RE than in SE using the CS-NaOCl-SSL system. This may indicate that the water matrix is not only scavenging radicals but also reacts with the oxidants (Ksibi 2006).

The possibility to take advantage of the sulfate radical formation to accelerate the reaction has been reported for oxidation processes based on sulfate radicals (Wu *et al.* 2015), and UV photolysis (Zhang *et al.* 2017). However, since this ion was in a similar concentration in both SE and RE, differences between the water matrices may be related to concentrations of the anions Cl^- and NO_3^-, which are seven and five times higher, respectively, in RE than SE. On this subject, reports pointed out that the presence of these ions represents a diminution of the degradation rate in AOPs like the UV/H_2O_2 process (Gultekin & Ince 2004) and photo-Fenton process using zero-valent iron (Gomathi Devi *et al.* 2012) or Fe-EDDS complex (Soriano-Molina *et al.* 2019). Nevertheless, there are no reports about the effect of ions present in the water matrix on the kinetics and degradation efficiency of MP using the solar NaOCl/Fe process.

Thus, calculating the kinetic constants for TBZ degradation (Table 4), it is evident that differences between water matrices are near to 30% in the CS-H_2O_2-SSL system, while the CS-NaOCl-SSL system has a difference for TBZ degradation of only 5%. That shows that the ionic concentration has a more important effect on the system whose oxidant is H_2O_2 in comparison to NaOCl. Moreover, results show that SE can be used as a tool to evaluate the performance of the process in real conditions under controlled conditions, but verification in RE is needed.

On the other hand, the values obtained for the CS-NaOCl-SSL system are one order of magnitude faster than CS-H_2O_2-SSL, and the same tendency is followed by the oxidant consumption, indicating that the use of NaOCl instead to H_2O_2 increases considerably the reaction rate.

In this regard, TBZ degradation in synthetic effluents have been reported using a homogeneous photo-Fenton process at both acidic (Rivas *et al.* 2015) and neutral pH (iron additions) (Carra *et al.* 2014). TBZ was fully degraded in 30 and 45 min, respectively; this time is significantly longer in comparison with the CS-NaOCl-SSL system.

The comparison between homogeneous photo-Fenton and the CS-NaOCl-SSL system opens a debate about which environmental impact is more important to avoid. On one hand, operation at both acidic pH implies the acidification and neutralization of the effluent before discharge into the environment (Papoutsakis *et al.* 2015); then, the addition of iron means that this catalyst turns into waste (Rizzo *et al.* 2019), while the extension of reaction times involves high energy consumption. But since the CS-NaOCl-SSL system complies with operation at neutral pH, short reaction time, and the feasibility to incorporate an industrial waste as an iron catalyst, such a process could be the key to diminishing the impacts of MP degradation by Fenton processes.

CONCLUSIONS

Complete TBZ degradation was achieved in three water matrices: distilled water, synthetic secondary effluent, and real secondary effluent of WWTP, by the use of two photo-assisted advanced oxidation processes: CS-H_2O_2-SSL and CS-NaOCl-SSL, separately. We present for the first time the effect of water matrix on the pollutant degradation and the kinetic constants of TBZ degradation using these systems in a comparative way.

Optimum operation conditions were determined in distilled water: $TBZ_0 = 7.36$ mg/L, 1.11 g CS /L, and 50 mg H_2O_2/L or 98 mg NaOCl/L. Results showed up to 90% TBZ degradation at 5 and 60 min when the oxidants were NaOCl and H_2O_2,

Table 4 | Results of the first-order kinetics for TBZ degradation and oxidant consumption

	TBZ_D				H_2O_2		NaOCl	
	CS-H_2O_2-SSL		CS-NaOCl-SSL		CS-H_2O_2-SSL		CS-NaOCl-SSL	
Water matrix	K_{TBZ_D} (1/min)	R^2	K_{TBZ_D} (1/min)	R^2	$K_{H_2O_2}$ (1/min)	R^2	K_{NaOCl} (1/min)	R^2
SE	0.024	0.99	0.365	1.00	0.008	0.96	0.237	0.97
RE	0.016	1.00	0.385	0.99	0.011	0.94	0.379	0.96

respectively. Reaction time differences are related to the type and quantity of radical species formed for each system. In the CS-NaOCl-SSL system, the formation of strong chlorine radicals like $Cl^{\bullet}$ (2.4 eV) and $Cl_2^{\bullet -}$ (2.0 eV) besides $HO^{\bullet}$ radical improved the rate of pollutant degradation, in comparison with the rate for the photo-Fenton-like reaction. Thus, in the CS-H_2O_2-SSL system, the presence of hydroxyl radical ($HO^{\bullet}$) is mainly responsible for the reaction performance, and its speed is strongly linked to the mass transfer of the heterogeneous system.

Slight differences in TBZ degradation efficiency were observed during five reuse cycles, showing that for the CS-H_2O_2-SSL system, a depletion of 80 ± 3% can be achieved in the same reaction time, 45 min, while at 5 min, an efficiency of 90 ± 1% was achieved using the CS-NaOCl-SSL system, regardless of the number of times that CS had been used (one to five). This means that CS is a chemically stable iron catalyst.

Finally, both processes were tested in SE and RE to observe the scavenger effect of the water matrix. Cl^- and NO_3^- concentrations were seven and five times higher, respectively, in RE than in SE. Results highlighted that the TBZ degradation in RE was slower than in SE for the heterogeneous photo-Fenton-like process (CS-H_2O_2-SSL), while the heterogeneous photo-NaOCl/Fe process was scarcely affected. In this way, if NaOCl was used instead, 94% TBZ degradation was reached at 10 min in both matrices, while for the CS-H_2O_2-SSL system TBZ degradation had values of 88 and 77% for SE and RE, respectively, at 90 min. It implies differences between the kinetic constants of 30 and 5% between RE and SE for the system oxidized by H_2O_2 and NaOCl, respectively.

Hence, as the CS-NaOCl-SSL system achieves complete degradation quickly and is applicable at neutral pH, is not greatly affected by ion concentrations and the iron catalyst is an industrial waste, this process looks like a feasible alternative for MP degradation, which deserves to be studied in depth in further work.

ACKNOWLEDGEMENTS

Reyna García Estrada acknowledges CONACYT for her Ph.D. scholarship. Sandra Arzate thanks DGAPA for her postdoctoral fellowship. The authors acknowledge the financial support granted by PAPIIT, UNAM (IT100921). Authors are also grateful to MSc. Leticia García Montes de Oca for the HPLC analysis.

DATA AVAILABILITY STATEMENT

All relevant data are included in the paper or its Supplementary Information.

CONFLICT OF INTEREST

The authors declare there is no conflict.

REFERENCES

Ahmadi, A., Zarei, M., Hassani, A., Ebratkhahan, M. & Olad, A. 2021 Facile synthesis of iron(II) doped carbonaceous aerogel as a three-dimensional cathode and its excellent performance in electro-Fenton degradation of ceftazidime from water solution. *Separation and Purification Technology* **278** (June), 119559. https://doi.org/10.1016/j.seppur.2021.119559.

Almanza, R. & López, S. 1978 Total solar radiation in Mexico using sunshine hours and meteorological data. *Solar Energy* **21** (5), 441–448. Available from: https://www.sciencedirect.com/science/article/pii/0038092X78901780?via%3Dihub.

Ameta, R., Chohadia, A. K., Jain, A. & Punjabi, P. B. 2018 Fenton and Photo-Fenton Processes. pp. 49–87 in Advanced Oxidation Processes for Waste Water Treatment, edited by Ameta, S. C. & Ameta, R. Academic Press.

Armstronga, D. A., Huie, R. E., Lymar, S., Koppenol, W. H., Merényi, G., Neta, P., Stanbury, D. M., Steenken, S. & Wardman, P. 2013 Standard electrode potentials involving radicals in aqueous solution: inorganic radicals. *BioInorganic Reaction Mechanisms* **9** (1–4), 59–61.

Arzate-Salgado, S.-Y., Morales-Pérez, A.-A., Solís-López, M. & Ramírez-Zamora, R.-M. 2016 Evaluation of metallurgical slag as a Fenton-type photocatalyst for the degradation of an emerging pollutant: diclofenac. *Catalysis Today* **266**, 126–135.

ASTM 1999 *ASTM D1193–99e1 Standard Specification for Reagent Water*. Available from: https://www.astm.org/DATABASE.CART/HISTORICAL/D1193-99E1.htm.

AWWA/APHA/WEF 2012 In: *Standard Methods for the Examination of Water and Wastewater* (Rice, E. W., Baird, R. B., Eaton, A. D. & Clesceri, L. S. C., eds). American Public Health Association, American Water Works Association, and Water Environment Federation, USA. Available from: https://www.techstreet.com/standards/standard-methods-for-the-examination-of-water-and-wastewater-22nd-edition-out-of-print?product_id=1817564.

Behin, J., Akbari, A., Mahmoudi, M. & Khajeh, M. 2017 Sodium hypochlorite as an alternative to hydrogen peroxide in Fenton process for industrial scale. *Water Research* **121**, 120–128. Available from: https://www.sciencedirect.com/science/article/abs/pii/S0043135417303743?via%3Dihub (accessed 20 December 2019).

Bel Hadjltaief, H., Da Costa, P., Beaunier, P., Gálvez, M. E. & Ben Zina, M. 2014 Fe-clay-plate as a heterogeneous catalyst in photo-Fenton oxidation of phenol as probe molecule for water treatment. *Applied Clay Science* **91–92**, 46–54.

Bernabeu, A., Vercher, R. F., Santos-Juanes, L., Simón, P. J., Lardín, C., Martínez, M. A., Vicente, J. A., González, R., Llosá, C., Arques, A. & Amat, A. M. 2011 Solar photocatalysis as a tertiary treatment to remove emerging pollutants from wastewater treatment plant effluents. *Catalysis Today* **161**, 235–240.

Bin, R., Mun, K., Wei, C., Pan, G. T., Yang, T. C. K. K., Ching, J., Lee, R. B., Lee, K. M., Lai, C. W., Pan, G. T., Yang, T. C. K. K. & Juan, J. C. 2018 The relationship between iron and Ilmenite for photocatalyst degradation. *Advanced Powder Technology* **29** (8), 1779–1786. https://doi.org/10.1016/j.apt.2018.04.013.

Cabrera Reina, A., Casas López, J. L., Maldonado Rubio, M. I., Santos-Juanes Jordá, L., García Sánchez, J. L. & Sánchez Pérez, J. A. 2014 Effects of environmental variables on the photo-Fenton plant design. *Chemical Engineering Journal* **237**, 469–477. http://dx.doi.org/10.1016/j.cej.2013.10.046 (accessed 24 July 2017).

Calza, P., Baudino, S., Aigotti, R., Baiocchi, C. & Pelizzetti, E. 2003 Ion trap tandem mass spectrometric identification of thiabendazole phototransformation products on titanium dioxide. *Journal of Chromatography A* **984** (1), 59–66.

Carmalin, S. A. & Eder, C. L. 2018 Removal of emerging contaminants from the environment by adsorption. *Ecotoxicology and Environmental Safety* **150** (December 2017), 1–17. https://doi.org/10.1016/j.ecoenv.2017.12.026.

Carra, I., Malato, S., Jiménez, M., Maldonado, M. I. & Sánchez Pérez, J. A. 2014 Microcontaminant removal by solar photo-Fenton at natural pH run with sequential and continuous iron additions. *Chemical Engineering Journal* **235**, 132–140. Available from: http://linkinghub.elsevier.com/retrieve/pii/S138589471301200X.

Carraro, P. M., Benzaquén, T. B., Alfano, O. M., Oliva, M. I. & Eimer, G. A. 2018 Advanced oxidation technologies to remove endocrine disruptors in water effluents based on zinc supported mesoporous catalysts. *Revista Mexicana de Ingeniería Quimica* **17** (3), 1135–1146.

Contreras-Bustos, R., Cárdenas Mijangos, J., Decoir-Espinoza, A., Rodríguez-García, A., Montoya-Herrera, L. & Jiménez-Becerril, J. 2019 Treatment of wastewater from the petrochemical industry by chemical Fenton process. *Revista Mexicana de Ingeniería Química* **19** (1), 523–532.

da Costa, E. P., Bottrel, S. E. C., Starling, M. C. V. M., Leão, M. M. D. & Amorim, C. C. 2019 Degradation of carbendazim in water via photo-Fenton in Raceway Pond Reactor: assessment of acute toxicity and transformation products. *Environmental Science and Pollution Research* **26** (5), 4324–4336. Available from: https://link.springer.com/article/10.1007/s11356-018-2130-z#citeas.

De la Obra, I., Ponce-Robles, L., Miralles-Cuevas, S., Oller, I., Malato, S. & Sánchez Pérez, J. A. 2017 Microcontaminant removal in secondary effluents by solar photo-Fenton at circumneutral pH in raceway pond reactors. *Catalysis Today* **287**, 10–14.

García-Estrada, R., Esteban García, B., Ramírez-Zamora, R. M. & Sánchez Pérez, J. A. 2020 Micropollutant degradation by the heterogeneous solar photo-Fenton process at circumneutral pH using copper slag. *Journal of Water Process Engineering* **38**, 101562. https://doi.org/10.1016/j.jwpe.2020.101562.

García-Muñoz, P., Pliego, G., Zazo, J. A., Bahamonde, A. & Casas, J. A. 2016 Ilmenite ($FeTiO_3$) as low cost catalyst for advanced oxidation processes. *Journal of Environmental Chemical Engineering* **4** (1), 542–548. https://doi.org/10.1016/j.jece.2015.11.037.

Georgiou, D., Melidis, P., Aivasidis, A. & Gimouhopoulos, K. 2002 Degradation of azo-reactive dyes by ultraviolet radiation in the presence of hydrogen peroxide. *Dyes and Pigments* **52** (2), 69–78.

Ghanbari, F., Zirrahi, F., Olfati, D., Gohari, F. & Hassani, A. 2020 TiO_2 nanoparticles removal by electrocoagulation using iron electrodes: catalytic activity of electrochemical sludge for the degradation of emerging pollutant. *Journal of Molecular Liquids* **310**, 113217. https://doi.org/10.1016/j.molliq.2020.113217.

Gomathi Devi, L., Girish Kumar, S., Mohan Reddy, K. & Munikrishnappa, C. 2012 Effect of various inorganic anions on the degradation of Congo Red, a di azo dye, by the photo-assisted Fenton process using zero-valent metallic iron as a catalyst. *Desalination and Water Treatment* **4** (1–3), 294–305. https://www.tandfonline.com/doi/pdf/10.5004/dwt.2009.478?needAccess = true.

Gualda-Alonso, E., Soriano-Molina, P., López, J. L. C., Sánchez, J. L. G., Plaza-Bolaños, P., Agüera, A. & Pérez, J. A. S. 2022 Large-scale raceway pond reactor for CEC removal from municipal WWTP effluents by solar photo-Fenton. *Applied Catalysis B: Environmental* 121908. Available from: https://linkinghub.elsevier.com/retrieve/pii/S0926337322008499 (accessed 5 September 2022).

Gultekin, I. & Ince, N. H. 2004 Degradation of reactive Azo Dyes by UV/H_2O_2: impact of radical scavengers. *Journal of Environmental Science and Health – Part A Toxic/Hazardous Substances and Environmental Engineering* **39** (4), 1069–1081.

Guo, K., Wu, Z., Shang, C., Yao, B., Hou, S., Yang, X., Song, W. & Fang, J. 2017 Radical chemistry and structural relationships of PPCP degradation by UV/Chlorine treatment in simulated drinking water. *Environmental Science and Technology* **51** (18), 10431–10439.

Hassani, A., Krishnan, S., Scaria, J., Eghbali, P. & Nidheesh, P. V. 2021 Z-scheme photocatalysts for visible-light-driven pollutants degradation: a review on recent advancements. *Current Opinion in Solid State and Materials Science* **25** (5), 100941. https://doi.org/10.1016/j.cossms.2021.100941.

Ji, Y., Zhou, L., Ferronato, C., Salvador, A., Yang, X. & Chovelon, J. M. 2013 Degradation of sunscreen agent 2-phenylbenzimidazole-5-sulfonic acid by TiO_2 photocatalysis: kinetics, photoproducts and comparison to structurally related compounds. *Applied Catalysis B: Environmental* **140–141**, 457–467. http://dx.doi.org/10.1016/j.apcatb.2013.04.046.

Kim, B. S., Jo, S. K., Shin, D., Lee, J. C. & Jeong, S. B. 2013 A physico-chemical separation process for upgrading iron from waste copper slag. *International Journal of Mineral Processing* **124**, 124–127. http://dx.doi.org/10.1016/j.minpro.2013.05.009.

Klamerth, N., Miranda, N., Malato, S., Agüera, A., Fernández-Alba, A. R., Maldonado, M. I. & Coronado, J. M. 2009 Degradation of emerging contaminants at low concentrations in MWTPs effluents with mild solar photo-Fenton and TiO_2. *Catalysis Today* **144** (1–2), 124–130. Available from: http://www.sciencedirect.com/science/article/pii/S0920586109000431 (accessed 14 April 2016).

Klamerth, N., Rizzo, L., Malato, S., Maldonado, M. I., Agüera, A. & Fernández-Alba, A. R. 2010 Degradation of fifteen emerging contaminants at microg L(-1) initial concentrations by mild solar photo-Fenton in MWTP effluents. *Water Research* **44** (2), 545–554. Available from: http://www.ncbi.nlm.nih.gov/pubmed/19853272 (accessed 8 November 2013).

Kong, X., Jiang, J., Ma, J., Yang, Y., Liu, W. & Liu, Y. 2016 Degradation of atrazine by UV/chlorine: efficiency, influencing factors, and products. *Water Research* **90**, 15–23.

Ksibi, M. 2006 Chemical oxidation with hydrogen peroxide for domestic wastewater treatment. *Chemical Engineering Journal* **119** (2–3), 161–165.

Lado Ribeiro, A. R., Moreira, N. F. F., Li Puma, G. & Silva, A. M. T. 2019 Impact of water matrix on the removal of micropollutants by advanced oxidation technologies. *Chemical Engineering Journal* **363** (October 2018), 155–173. Available from: https://www.sciencedirect.com/science/article/pii/S1385894719300968 (accessed 25 March 2019).

Larralde, A. L., Onna, D., Fuentes, K. M., Sileo, E. E., Hojamberdiev, M. & Aldabe Bilmes, S. 2019 Heterogeneous photo-Fenton process mediated by Sn-substituted goethites with altered OH-surface density. *Journal of Photochemistry and Photobiology A: Chemistry* **381** (May), 111856. https://doi.org/10.1016/j.jphotochem.2019.111856.

Lima, M. J., Silva, C. G., Silva, A. M. T., Lopes, J. C. B., Dias, M. M. & Faria, J. L. 2017 Homogeneous and heterogeneous photo-Fenton degradation of antibiotics using an innovative static mixer photoreactor. *Chemical Engineering Journal* **310**, 342–351. Available from: https://www.sciencedirect.com/science/article/pii/S1385894716304715#b0235 (accessed 1 December 2019).

Loures, C., Alcântara, M. & Filho, H. 2013 Advanced oxidative degradation processes: fundamentals and applications. *International Review of Chemical Engineering* **5** (March), 102–120. Available from: http://www.researchgate.net/publication/236735665_Advanced_Oxidative_Degradation_Processes_Fundamentals_and_Applications/file/e0b495192826d14e33.pdf.

Murthy, N. B. K., Moza, P. N., Hustert, K., Raghu, K. & Kettrup, A. 1996 Photolysis of thiabendazole in aqueous solution and in the presence of fulvic and humic acids. *Chemosphere* **33** (10), 1915–1920.

Neyens, E. & Baeyens, J. 2003 A review of classic Fenton's peroxidation as an advanced oxidation technique. *Journal of Hazardous Materials* **98** (1–3), 33–50.

Nowell, L. H. & Hoigni, J. U. R. G. 1992 Photolysis of aqueous chlorine at sunlight. *Production* **26** (5), 593–598. Available from: https://www.sciencedirect.com/science/article/pii/004313549290232S.

OECD 2001 *Simulation Test – Aerobic Sewage Treatment 303A*. Available from: http://biotecnologiebt.com/guide/OECD_227.pdf.

Omri, A., Hamza, W. & Benzina, M. 2020 Photo-Fenton oxidation and mineralization of methyl orange using Fe-sand as effective heterogeneous catalyst. *Journal of Photochemistry and Photobiology A: Chemistry* **393**, 112444.

Papoutsakis, S., Brites-Nóbrega, F. F., Pulgarin, C. & Malato, S. 2015 Benefits and limitations of using Fe(III)-EDDS for the treatment of highly contaminated water at near-neutral pH. *Journal of Photochemistry and Photobiology A: Chemistry* **303**, 1–7. Available from: http://www.sciencedirect.com/science/article/pii/S1010603015000398 (accessed 20 April 2017).

Pescod, M. B. 1992 Agricultural use of sewage sludge. In: *Wastewater Treatment and Use in Agriculture – FAO Irrigation and Drainage Paper 47*. Food and Agriculture Organization of the United Nations, 6.1. Available from: http://www.fao.org/3/t0551e/t0551e03.htm (accessed 22 May 2020).

Pignatello, J. J., Oliveros, E. & MacKay, A. 2006 Advanced oxidation processes for organic contaminant destruction based on the Fenton reaction and related chemistry. *Critical Reviews in Environmental Science and Technology* **36** (1), 1–84.

Portilla-Sangabriel, M., Arzate, S., Macías-Vargas, J. A. & Ramírez-Zamora, R. M. 2021 Assessment of the use of NaClO as an alternative to H_2O_2 in the oxidant-titanium ore-simulated solar light system for thiabendazole degradation. *Topics in Catalysis* **64**, 181–193. https://doi.org/10.1007/s11244-020-01388-8.

Portilla Sangabriel, M., Martínez Piernas, A. B., Agüera, A., Arzate, S., Sánchez-Pérez, J. A. & Ramírez-Zamora, R. M. 2022 Degradation of thiabendazole and its transformation products by two photo-assisted iron-based-processes in a raceway pond reactor. *Topics in Catalysis* **65**, 1113–1127. https://doi.org/10.1007/s11244-022-01638-x.

Rivas, G., Carra, I., García Sánchez, J. L., Casas López, J. L., Malato, S. & Sánchez Pérez, J. A. 2015 Modelling of the operation of raceway pond reactors for micropollutant removal by solar photo-Fenton as a function of photon absorption. *Applied Catalysis B: Environmental* **178**, 210–217.

Rizzo, L., Malato, S., Antakyali, D., Beretsou, V. G., Đolić, M. B., Gernjak, W., Heath, E., Ivancev-Tumbas, I., Karaolia, P., Lado Ribeiro, A. R., Mascolo, G., McArdell, C. S., Schaar, H., Silva, A. M. T. & Fatta-Kassinos, D. 2019 Consolidated vs new advanced treatment methods for the removal of contaminants of emerging concern from urban wastewater. *Science of The Total Environment* **655**, 986–1008. Available from: https://www.sciencedirect.com/science/article/pii/S0048969718346229 (accessed 25 June 2019).

Sandoval-Gonález, A., Álvarez-Gallegos, A., Hernández, J. A. & Silva-Martínez, S. 2021 Degradation of sucralose present in Splenda® sweetener by TiO_2 photocatalysis assisted with photo-Fenton. *Revista Mexicana de Ingeniería Química* **20** (1), 213–226.

Sirtori, C., Agüera, A., Carra, I. & Sanchéz Pérez, J. A. 2014 Identification and monitoring of thiabendazole transformation products in water during Fenton degradation by LC-QTOF-MS. *Analytical and Bioanalytical Chemistry* **406** (22), 5323–5337.

Solís-López, M., Durán-Moreno, A., Rigas, F., Morales, A. A., Navarrete, M. & Ramírez-Zamora, R. M. 2014 *Assessment of Copper Slag as A Sustainable Fenton-Type Photocatalyst for Water Disinfection*. Elsevier Inc. Available from: http://linkinghub.elsevier.com/retrieve/pii/B9780124116450000092

Soriano-Molina, P., Plaza-Bolaños, P., Lorenzo, A., Agüera, A., García Sánchez, J. L., Malato, S. & Sánchez Pérez, J. A. 2019 Assessment of solar raceway pond reactors for removal of contaminants of emerging concern by photo-Fenton at circumneutral pH from very different municipal wastewater effluents. *Chemical Engineering Journal* **366**, 141–149. Available from: https://www.sciencedirect.com/science/article/pii/S1385894719303043 (accessed 9 February 2019).

Tokumura, M., Sugawara, A., Raknuzzaman, M., Habibullah-Al-Mamun, M. & Masunaga, S. 2016 Comprehensive study on effects of water matrices on removal of pharmaceuticals by three different kinds of advanced oxidation processes. *Chemosphere* **159**, 317–325.

Wu, Y., Bianco, A., Brigante, M., Dong, W., De Sainte-Claire, P., Hanna, K. & Mailhot, G. 2015 Sulfate radical photogeneration using Fe-EDDS: influence of critical parameters and naturally occurring scavengers. *Environmental Science and Technology* **49** (24), 14343–14349.

Zhang, Y., Zhang, J., Xiao, Y., Chang, V. W. C. & Lim, T. T. 2017 Direct and indirect photodegradation pathways of cytostatic drugs under UV germicidal irradiation: process kinetics and influences of water matrix species and oxidant dosing. *Journal of Hazardous Materials* **324**, 481–488. http://dx.doi.org/10.1016/j.jhazmat.2016.11.016.

Zhang, M., Dong, H., Zhao, L., Wang, D. & Meng, D. 2019 A review on Fenton process for organic wastewater treatment based on optimization perspective. *Science of The Total Environment* **670**, 110–121. Available from: https://www.sciencedirect.com/science/article/pii/S0048969719311684 (accessed 21 March 2019).

Zhu, Y., Zhu, R., Xi, Y., Zhu, J., Zhu, G. & He, H. 2019 Strategies for enhancing the heterogeneous Fenton catalytic reactivity: a review. *Applied Catalysis B: Environmental* **255**, 117739. https://doi.org/10.1016/j.apcatb.2019.05.041.

First received 26 September 2022; accepted in revised form 9 December 2022. Available online 22 December 2022